Cell Biochem Biophys (2013) 67:461–476
DOI 10.1007/s12013-012-9367-9

ORIGINAL PAPER

Oxidative Stress and Dermal Toxicity of Iron Oxide Nanoparticles In Vitro

Ashley R. Murray · Elena Kisin · Alfred Inman · Shih-Houng Young · Mamoun Muhammed · Terrance Burks · Abdusalam Uheida · Alexey Tkach · Micah Waltz · Vincent Castranova · Bengt Fadeel · Valerian E. Kagan · Jim E. Riviere · Nancy Monteiro-Riviere · Anna A. Shvedova

Published online: 5 June 2012

Abstract A number of commercially available metal/metal oxide nanoparticles (NPs) such as superparamagnetic iron oxide (SPION) are utilized by the medical field for a wide variety of applications. These NPs may able to induce dermal toxicity via their physical nature and reactive surface properties. We hypothesize that SPION may be toxic to skin via the ability of particles to be internalized and thereby initiate oxidative stress, inducing redox-sensitive transcription factors affecting/leading to inflammation. Due to the skin's susceptibility to UV radiation, it is also of importance to address the combined effect of UVB and NPs co-exposure. To test this hypothesis, the effects of dextran-coated SPION of different sizes (15–50 nm) and manufacturers (Micro-Mod, Rostock-Warnemunde, Germany and KTH-Royal Institute of Technology, Stockholm, Sweden) were evaluated in two cell lines: normal human epidermal keratinocytes (HEK) and murine epidermal cells (JB6 P^+). HEK cells exposed to 20 nm (KTH and MicroMod) had a decrease in viability, while the 15 and 50 nm particles were not cytotoxic. HEK cells were also capable of internalizing the KTH particles (15 and 20 nm) but not the MicroMod SPION (20 and 50 nm). IL-8 and IL-6 were also elevated in HEK cells following exposure to SPION. Exposure of JB6 P^+ cells to all SPIONs evaluated resulted in activation of AP-1. Exposure to SPION alone was not sufficient to induce NF-κB activation; however, co-exposure with UVB resulted in significant NF-κB induction in cells exposed to 15 and 20 nm KTH SPION and 50 nm MicroMod particles. Pre-exposure of JB6 P^+ cells to UVB followed by NPs induced a significant depletion of glutathione, release of cytokines, and cell damage as assessed by release of lactate dehydrogenase. Altogether, these data indicate that co-exposure to UVB and SPIONs was associated with induction of oxidative stress and release of inflammatory mediators. These results verify the need to thoroughly evaluate the adverse effects of UVB when evaluating dermal toxicity of engineered NPs on skin.

Keywords Nanoparticles · Skin exposure · Ultraviolet radiation · Iron oxide

A. R. Murray · E. Kisin · S.-H. Young · A. Tkach · V. Castranova · A. A. Shvedova (✉)
Pathology and Physiology Research Branch, Health Effects Laboratory Division, National Institute for Occupational Safety and Health (NIOSH), M/L 2015, 1095 Willowdale Road, Morgantown, WV 26505, USA
e-mail: ats1@cdc.gov

A. R. Murray · M. Waltz · A. A. Shvedova
Department of Physiology and Pharmacology, West Virginia University, Morgantown, WV, USA

A. Inman · J. E. Riviere · N. Monteiro-Riviere
Center for Chemical Toxicology Research and Pharmacokinetics, North Carolina State University, Raleigh, NC, USA

M. Muhammed · T. Burks · A. Uheida
Functional Materials Division, Royal Institute of Technology (KTH), Kista, Stockholm, Sweden

B. Fadeel
Division of Molecular Toxicology, Institute of Environmental Medicine, Karolinska Institutet, Stockholm, Sweden

V. E. Kagan
Department of Environmental and Occupational Health, Center for Free Radical and Antioxidant Health, University of Pittsburgh, Pittsburgh, PA, USA

Introduction

Nanotechnology is a rapidly emerging field resulting in the discovery of unique materials with a variety of applications

from electronics to engineered tissues [1]. Superparamagnetic iron oxide nanoparticles (SPION) have a variety of uses in the biomedical field [2]. Biocompatible SPION particles have been utilized for a number of in vivo applications such as magnetic resonance imaging contrast agents [3–7], targeted drug delivery systems [8, 9], hyperthermia treatment of tumors [10–12], and wound healing [13].

SPIONs can be functionalized with a variety of surface coatings and targeting ligands to increase visualization/detection of tumors [14–16] as well as visualization of a number of biological processes (i.e., apoptosis, cell trafficking, and gene expression [17–20]). Variations in particle size (with hydrodynamic diameter from 10 to 500 nm [21]) and surface coatings affect blood half-life, biodistribution, and particle uptake [22–25]. Various coatings allow the functional properties of the nanoparticles (NPs) to be customized for a number of clinical applications [26]. The most common coatings are derivatives of dextran, albumin, silicones, polyethylene glycol (PEG) [26], polyethylene oxide (PEO), poloxamers, and polyoxamines [27]. Biological applications typically utilize SPION coated with a water soluble polymer such as dextran or PEG [28] which allows for greater dispersion. Dextran-coated SPIONs have shown the most promise because of their long half-life and low toxicity [26]. Introduction of these novel materials requires a thorough safety evaluation as well as an understanding of the impact of the nanomaterials on human health.

Dermal exposure is a potential route of exposure to SPION due to their production and novel use in wound healing [13]. Conjugation of NPs and therapeutic drugs has the potential to enhance the effectiveness via protection of these drugs from their natural inhibitors, such as enzymatic degradation [13]. One such potential use is the conjugation of thrombin to iron oxide NPs for utilization in the promotion of wound healing as it is necessary for the conversion of fibrinogen to fibrin and whose action is critical and necessary for the early and late stages of wound healing [13]. SPION have also been shown to have adverse effects to dermal fibroblasts [26]. Currently, there is limited literature available evaluating the toxic effects of SPIONs to the skin and skin cells.

Another important aspect to consider when evaluating dermal particle toxicity is the susceptibility of the skin to ultraviolet radiation (UVR). Solar radiation reaching the earth consists mainly of UVA (315–400 nm) and UVB (280–315 nm) light and is a major environmental and occupational exposure risk. As a result of reduction of the stratospheric ozone layer, there has been an increase in dermal exposure to UVR accompanied by an increase in the development of associated skin diseases [27, 28]. UVR has been shown to be a source of exogenous and environmental reactive oxygen species (ROS). ROS, such as superoxide anion, hydroxyl radical, hydrogen peroxide and molecular oxygen, are involved in cell proliferation, apoptosis, immune responses, and cell differentiation [29]. Overproduction of ROS can result in the development and progression of a variety of skin maladies in which inflammatory mediators are implicated [30]. Therefore, the ability of UVB to potentiate NP-induced toxicity should be considered.

Internalization of dextran-coated SPION particles can lead to the dextran shell being broken down resulting in particle chains and aggregates, which may influence cellular processes and viability [27, 31]. Our central hypothesis is that SPIONs may cause skin toxicity via particle uptake and induction of oxidative stress leading to activation of AP-1/NF-κB and cytokine release with enhancement of the toxic effect from UVB exposure (Scheme 1). To address these questions, the effects of SPIONs of different sizes and manufacturers were evaluated in normal human epidermal keratinocytes (HEK) and murine epidermal JB6 P^+ cells with or without UVB exposure. The ability of SPIONs to be taken into the cells and thereby induce cellular toxicity as well as oxidative stress in JB6 P^+ cells was assessed by evaluating cell damage as measured by lactate dehydrogenase (LDH), decreases in glutathione (GSH), as well as activation of AP-1 and NF-κB and release of inflammatory cytokines after exposure. The obtained data provide insight into potential mechanisms of dermal toxicity induced by exposure to SPION.

Materials and Methods

Chemicals

Fatty acid-free human serum albumin, sodium dodecyl sulfate, fetal bovine serum (FBS), GSH, and MTT were purchased from Sigma Chemicals Co. (St. Louis, MO). ThioGlo-1 was obtained from Covalent Inc. (Wobum, MA). Phosphate-buffered saline (PBS), alamar Blue and minimum essential medium (MEM) were purchased from Invitrogen Corporation (Carlsbad, CA). Luciferase Assay system was purchased from Promega Corporation (Madison, WI).

Particles

Dextran-coated SPION with primary particle sizes of 20 and 50 nm were obtained from MicroMod (Rostock-Warnemunde, Germany). 15 and 20 nm dextran-coated SPION were manufactured and obtained from KTH-Royal Institute of Technology (Stockholm, Sweden).

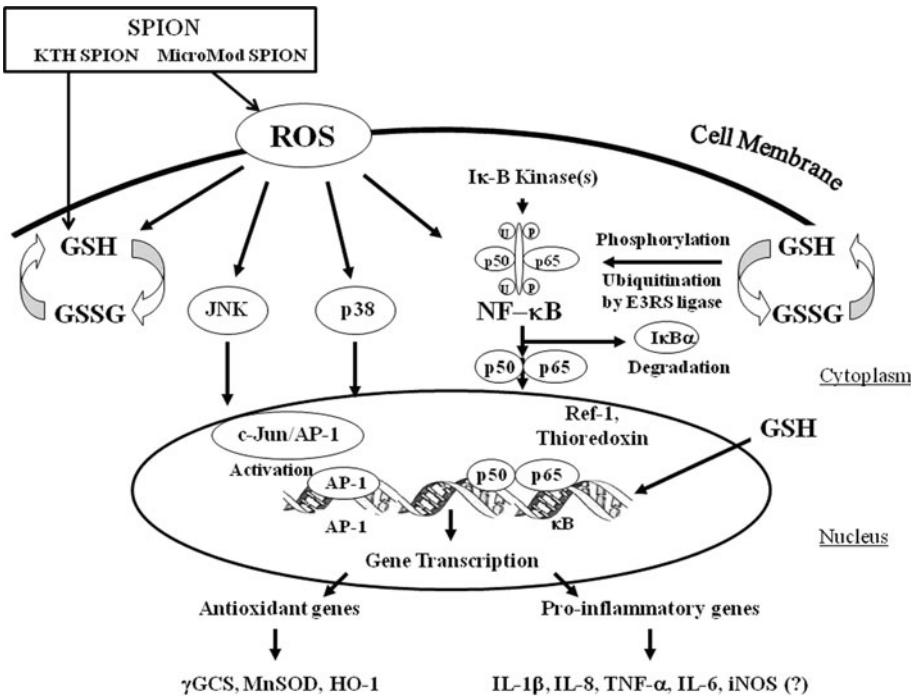

Scheme 1 SPIONs interaction with skin may induce skin toxicity via particle uptake and induction of oxidative stress leading to activation of AP-1/NF-κB and cytokine release with enhancement of the toxic effect resulting from UVB exposure

Synthesis of Dextran-Coated SPION

Analytical grade solutions of $FeCl_2$, $FeCl_3$, hydrochloric acid, ammonium hydroxide, and dextran were used. A stock solution of iron(III) and iron(II) in chloride media was prepared by dissolving the respective salts with deoxygenated 0.1 M HCl aqueous solution to a final concentration of 1 and 0.5 M. This solution was added to a deoxygenated solution containing 0.7 M NH_3 under mechanical stirring at 250 rpm. The particles were aged in the solution for about 45 min, decantated by magnetic settling, and washed with deoxygenated water three times. After the third wash, 10.9 g of dextran (Mw: 6000, 40,000, and 70,000 Da) was added to 45 ml of magnetite NPs. The SPION and the dextran were then mixed using Multi-Wrist Shaker for 24 h. The final product was placed into Spectra Pro MWCO 25,000 membrane for dialysis for 3 days, while changing the water every 3 h. The presence of dextran coating was then verified using FT-IR (Nicolet Instrument model Avatar-100 equipped with ATR diamond at 303 K) and size was verified by dynamic light scatter (DLS).

Transmission Electron Microscopy (TEM) of SPION

A small amount of suspended solution (3–5 drops) was added into a glass vial containing 10 ml of ultrapure water. The sample was sonicated (Vibra Cell, Newtown, CT) for 1 min to ensure the sample is well dispersed. One drop of the NP suspension was deposited onto a copper grid, which is coated with formvar and carbon. The sample was left to dry before the TEM analysis could be conducted. Moreover, to determine the particle size and its distribution, the images were processed using software "the Image J". 100 particle counts per sample were evaluated to determine and generate the average number of particle in dry form.

DLS Analysis

A small amount of suspended solution (3–5 drops) was added into a glass vial containing 10 ml of ultrapure water. The sample was sonicated (Vibra Cell, Newtown, CT) for 1 min to ensure the sample is well dispersed. Minimum amount of 1 ml of the sample (suspension) was placed into a quartz cuvette. The sample was analyzed using a Delsa NanoC DLS (Beckman Coulter, Brea, CA). The results from DLS are passed upon and reported in the form of maximum intensity peak because the algorithm used to determine the particle size is based upon intensity.

Fourier Transform Infra Red Spectroscopy (FTIR)

A small amount of suspended or powdered solution was placed onto the sample holder of the FTIR instrument (Avatar 360 FTIR; Thermo Fisher Scientific, Waltham, MA). The data are collected and reported in the form of spectra where the wave number ranges from 400 to 4,000 cm^{-1}. This technique is used to determine the functional groups of organic species, e.g., dextran, as well as the inorganic polymer iron oxide.

Normal HEK Cell Culture and SPION Exposure

Cryopreserved first pass HEK (Lonza; Basel, Switzerland) were seeded in 75-cm^2 flasks and grown to ~75 % confluency, harvested, and plated in the inner wells of 96-well plates at a concentration of 12,500 cells/well in 200 µl of KGM-2 medium. Medium was placed in the peripheral wells of the plate to stabilize plate temperature and minimize evaporation from the inner wells. The cells were grown for 18 h in a 5 % CO_2 atmosphere at 37 °C and exposed routinely to SPION. A stock solution of 400 µg/ml was prepared for each NP in the KGM-2 cell culture medium by briefly vortexing. SPION were placed in the wells ($n = 6$ wells/treatment) and the HEK were exposed for 24 h. Media from the treatments was harvested and stored at −80 °C for analysis of cytokines.

TEM of HEK Cells Following SPION Exposure

To study the uptake of the dextran-coated SPION into HEK, the cells were grown to 70 % confluency in 25-cm^2 flasks and exposed to 26 µg/cm^2 of SPION for 24 h. The HEK were harvested with trypsin/EDTA, rinsed in Hanks' Balanced Salt Solution (HBSS), and fixed with Trump's fixative. The cells were rinsed in 0.1 M phosphate buffer, embedded as a pellet in 3 % agar, and post-fixed in 1 % osmium tetroxide in 0.1 M phosphate buffer. The cells were briefly rinsed in distilled water, dehydrated through graded ethanols, cleared in acetone, and infiltrated and embedded in Spurr's resin. Thin sections (~800 Å) were mounted on copper grids and examined unstained on a FEI/Philips EM208S TEM.

JB6 P^+ Cell Culture and Co-exposure of UVB and SPION

Epidermal JB6 P^+ cells were utilized to study the effects of SPION on the AP-1 and NF-κB pathways involved in mediating inflammatory responses [32–36]. The JB6 family of mouse epidermal clonal genetic variants (P^+/P^-) provides a suitable model for studying critical gene regulation events. Tumor-promotion-sensitive JB6 P^+ cells respond irreversibly to phorbol esters, resulting in the induction of anchorage independent growth as well as tumorigenicity [34–36]. JB6 P^+ mouse epidermal cells were transfected with an AP-1-luciferase reporter plasmid (JB6/AP-1) or a NF-κB luciferase reporter plasmid (JB6/NF-κB). The cell line was a kind gift from the laboratory of Dr. Nancy Colburn (National Institutes of Health, Frederick, MD). The JB6 P^+ cells were cultured in Eagle's MEM containing 5 % fetal bovine serum and 2 mM L-glutamine. The cells were grown at 37 °C in a 5 % CO_2 atmosphere to reach 80 % confluency before exposure to SPION. Prior to NP exposure, one group of cells was exposed to 4 kJ/m^2 UVB radiation in MEM without phenol red and another group of cells remained under normal growth conditions in MEM without phenol red. To evaluate cytotoxicity and oxidative damage, cells were exposed to various concentrations of SPION (2.6, 5.2, 13, or 26 µg/cm^2) in MEM medium without phenol red for 24 h at 37° C. After incubation, cells were washed twice with PBS, pH 7.4, and harvested using a cell scraper. Cellular supernatants were collected and utilized for evaluation of release of LDH and cytokines. JB6 cell homogenates were prepared by freezing at −80 °C.

Viability Assessment of HEK and JB6 P^+ Cells Following Fe_3O_4 NP Exposure

Cell viability was assayed by two methods: MTT (Sigma/Aldrich; St. Louis, MI) and alamar Blue (Invitrogen; Carlsbad, CA). The MTT viability assay was used to determine cytotoxicity of SPION to HEK cells. After the treatment, medium was removed and the cells were incubated with MTT medium (0.5 mg/ml in KGM-2) for 3 h under cell culture conditions. The tetrazolium dye was extracted from the cells with isopropanol, transferred to a new plate, and the absorbance quantitated at 550 nm in a Multiskan RC plate reader (Labsystems; Kennett Square, PA). The raw values for all the assays were normalized by the controls and expressed as percent viability. The 96-well plates were centrifuged after the incubation to ensure that the NP did not interfere with the absorbance or fluorescence readings.

The viability of JB6 P^+ cells following exposure was evaluated using the alamar Blue bioassay, as described by Keane et al. [37]. Cells were incubated at 37 °C with 10 % alamar Blue (4 h). A fluorescence multiwell plate reader (CytoFluor Series 4000, PerSeptive Biosystems, Framingham, MA) with 530 nm excitation and 580 nm emission was then employed in the assay. The results are analyzed using CytoFluor Version 4.2.1 (PerSeptive Biosystems, Framingham, MA).

Due to potential interactions of the dextran-coated SPION with the viability assays, the UV/Visible spectrum was determined [38]. The NP were suspended in the assay medium in a 15-ml centrifuge tube, incubated under cell culture conditions for 3 h, and pelleted by centrifugation. The NPs in the MTT medium were rinsed and extracted with agitation. The extracted solution was transferred to quartz cuvettes and absorbance read at intervals from 300 to 700 nm on a UV–Vis spectrophotometer using the KGM-2 medium as the blank. The alamar Blue medium was transferred to a 96-well black plate and fluorescence read at intervals between 565 and 640 nm.

Production of Cytokines by HEK Cells

Human cytokines, IL-6, IL-8, and TNF-α, were quantified by multiplexing with the Bio-Plex suspension assay system (Bio-Rad Laboratories; Hercules, CA). Treatment and control media from the viability assays were incubated with the capture antibody (conjugated to bead), fluorescently labeled and analyzed. The cytokines were quantitated relative to a standard curve. The limit of detection for each cytokine is as follows: IL-8, 0.5 pg/ml; IL-1, 1.1 pg/ml; and TNF-α, 3.0 pg/ml. The data from each cytokine were normalized to viable cells.

LDH Activity

In order to assess cell damage induced by SPION exposure with or without UVB pre-treatment, LDH release was evaluated in the supernatant of exposed cells. The level of LDH in cellular supernatants of JB6 cells was assayed spectrophotometrically by monitoring the reduction of nicotinamide adenine dinucleotide at 340 nm in the presence of lactate using the LDH Reagent Set (Pointe Scientific, Lincoln Park, MI). LDH release was normalized to viable cells.

Fluorescence Assay of GSH

GSH concentration in JB6 P^+ cell homogenates was determined using ThioGlo-1, a maleimide reagent which produces a highly fluorescent product upon its reaction with sulfhydryl groups [39]. A standard curve was established by addition of GSH (0.04–2.0 μM) to 0.1 M phosphate buffer (pH 7.4) containing 10 μM ThioGlo-1. GSH content was estimated by an immediate fluorescence response registered upon addition of ThioGlo-1 to cell homogenates. A Shimadzu spectrofluorometer RF-5000 U (Shimadzu, Japan) was employed in the assay with excitation 388 nm and emission 500 nm. The data were acquired using an excitation slit of 1.5 nm and an emission slit of 5 nm. The fluorescence signals were exported from the spectrofluorometer using RF-5000 U PC Personal Fluorescence software (Shimadzu, Japan).

Assay of AP-1 and NF-κB Activity In Vitro

To study whether SPION exposure caused changes in AP-1 and NF-κB activities, JB6 P^+ cells (5×10^4 cells/ml) were cultured in 96-well plates (200 μl per well) in Eagle's MEM supplemented with 5 % fetal bovine serum plus 2 mM L-glutamine. Plates were incubated at 37 °C in a humidified atmosphere of 5 % CO_2. Twelve hours later, cells were cultured in MEM supplemented media with 0.1 % FBS (24 h) to minimize basal AP-1 and NF-κB activity. JB6 P^+ cells pre-exposed with/without UVB (4 kJ/m^2) were treated with SPION (2.6, 5.2, or 26 μg/cm^2) or vehicle (PBS). Following 24-h incubation with SPION, the cells were incubated with 200 μl of 1× lysis buffer provided by the manufacturer (Promega, Madison, WI) and the luciferase activity was measured using a luminometer (Monolight 2010, Analytical Luminescence Laboratory, San Diego, CA). The results are expressed as relative AP-1 or NF-κB activity compared to respective controls.

Production of Cytokines by JB6 P^+ Cells

Levels of the mouse inflammatory cytokines, IL-6, MCP-1, IFN-γ, TNF-α, and IL-12, were assayed in the cell supernatants with/without UVB and SPION exposure. The concentrations were determined using the BD Cytometric Bead Array, Mouse Inflammation kit (BD Biosciences, San Diego, CA). Six bead populations with distinct fluorescence intensities have been coated with capture antibodies specific for IL-6, IL-10, MCP-1, IFN-γ, TNF-α, and IL-12p70 proteins. The six bead populations are mixed together to form the BD™ CBA which is resolved in the FL3 channel of a flow cytometer. The sensitivity of the assay is 5–7.3 pg/ml. The data from each cytokine were normalized to viable cells.

Protein Assay

Total protein in cellular homogenates from JB6 P^+ mouse epidermal cells following exposure with/without UVB and SPION was evaluated using a Bio-Rad protein assay kit (Richmond, CA).

Statistics

Treatment-related differences were evaluated using two-way ANOVA, followed by pair-wise comparison using the Student–Newman–Keuls tests, as appropriate. Statistical significance was considered at $p < 0.05$.

Results

TEM and Size Distribution of SPION

TEM and DLS were utilized to determine the size distribution of SPION particles (Fig. 1). TEM analysis of KTH SPION (15 nm; Fig. 1a, e) found particles to be 15.0 ± 3.7 nm while the 20 nm particles (Fig. 1d, h) were 20.4 ± 7.5 nm. DLS evaluation of particles in water and cell culture media found the 15 nm KTH particles were 100 and 134 nm, respectively, while the 20 nm KTH particles were 111 and 160 nm, respectively (Table 1). MicroMod SPION (20 nm; Fig. 1c, g) were confirmed to be

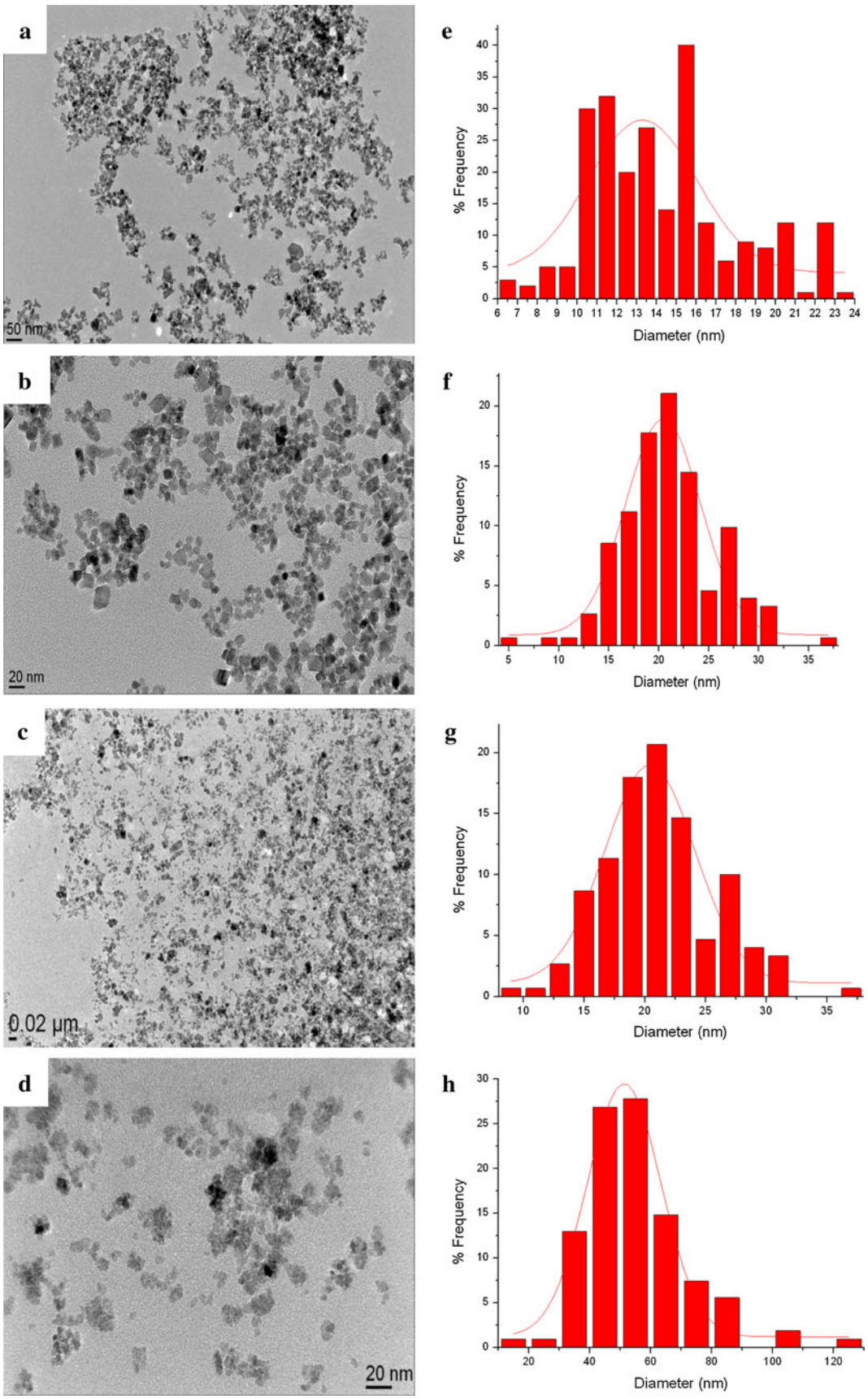
a
50 nm
b
20 nm
c
0.02 μm
d
20 nm
e
% Frequency
Diameter (nm)
f
% Frequency
Diameter (nm)
g
% Frequency
Diameter (nm)
h
% Frequency
Diameter (nm)

◀ **Fig. 1** TEM (**a**–**d**) and size distribution (**e**–**h**) of SPION: KTH SPION 15 nm (**a**, **e**) and 20 nm (**b**, **f**), MicroMod SPION 20 nm (**c**, **g**), and 50 nm (**d**, **h**)

Table 1 Particle size evaluation of SPION

SPION	Particle size (nm)		
	TEM	DLS	
		Water	Cell culture media
KTH SPION-dex lab made, 15 nm	15 ± 3.7	100	134
KTH SPION-dex lab made, 20 nm	20.4 ± 7.5	111	160
20 nm MicroMod nanomag-D-SPIO	21.1 ± 4.7	346	87
50 nm MicroMod nanomag-D-SPIO	54.9 ±16.6	428	103

21.1 ± 4.7 nm and the 50 nm particles (Fig. 1d, h) were determined to be 54.9 ± 16.6 nm. In water and cell culture media, the 20 nm MicroMod particles were 346 and 87 nm, respectively, while the 50 nm particles had a particle size of 428 and 160 nm, respectively (Table 1). Dextran coating of all the SPION particles was confirmed via FTIR.

Viability of HEK Following Exposure to Fe_3O_4 NPs (SPIONs)

The effects of metal oxide NPs on a number of cytotoxicity assays have been reported; therefore, UV/Visible is an evaluation of the cytotoxicity assays utilized in this study conducted to determine any interactions of the viability dyes (MTT and alamar Blue) with the test SPIONs. The results revealed that the absorbance and fluorescence values of the controls (no NP) are the same as the media containing the SPION (data not shown). This indicates little to no interaction of the SPION with the dyes of the viability assays.

Exposure of HEK cells to 20 nm MicroMod revealed a significant decrease (16 %) in viability following treatment with 26 μg/cm^2 SPION (Fig. 2a). 50 nm MicroMod (Fig. 2b) and 15 nm KTH SPION (Fig. 2c) did not induce cytotoxicity in HEK at the concentrations evaluated. The larger 20 nm KTH SPION (Fig. 2c) induced significant cytotoxicity with a 20–25 % reduction in viability at all concentrations evaluated (2.6–26 μg/cm^2).

Uptake of SPION by HEK

The control cells (no treatment) appear healthy, with no inclusions resembling the NP (Fig. 3a). Identifiable electron-dense MicroMod SPION were not observable within

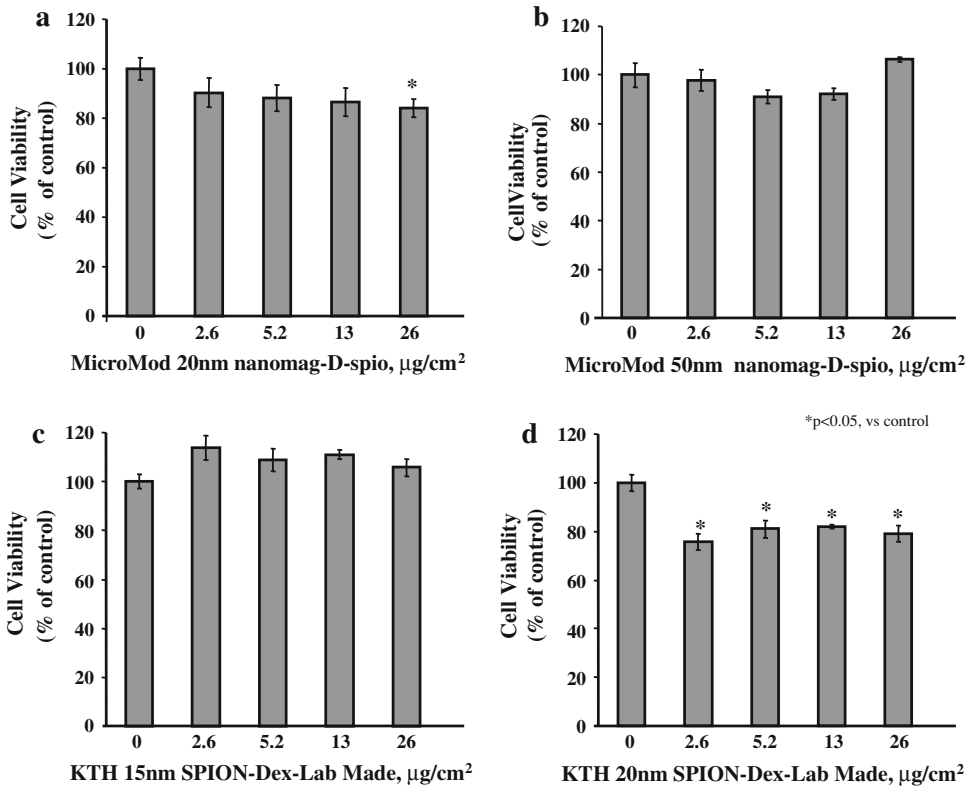

Fig. 2 Viability of HEK following exposure to SPION. **a** MicroMod 20 nm, **b** MicroMod 50 nm, **c** KTH 15 nm, **d** KTH 20 nm. Conditions: HEK cells (12,500 cells/well) were exposed to 2.6-, 5.2-, 13-, or 26-μg/cm^2 SPION ($n = 6$ wells/treatment) for 24 h at 37 °C. After the incubation, cells were washed twice with PBS (pH 7.4), and cell viability was determined by the MTT assay. Significance indicated by *$p < 0.05$ versus control

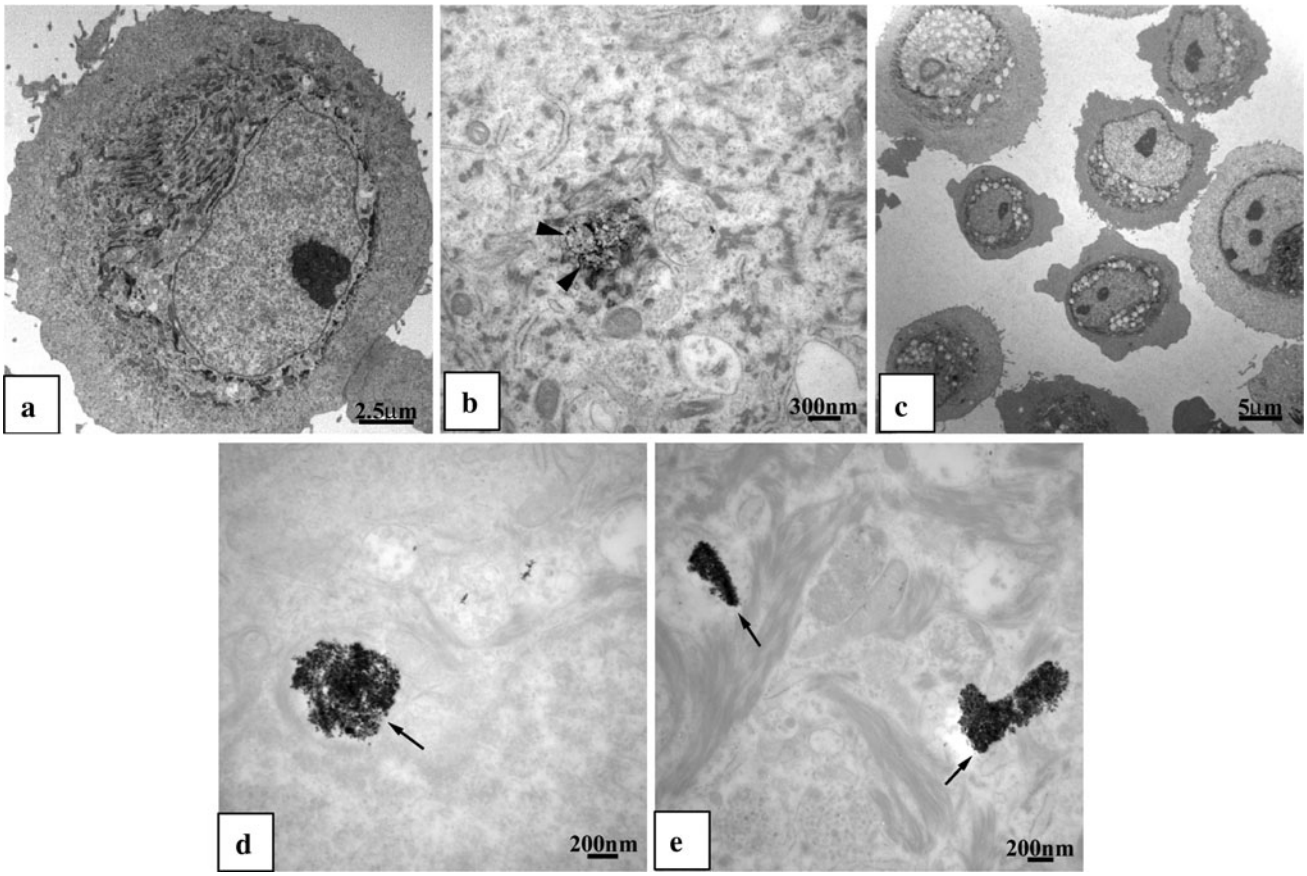

Fig. 3 TEM of HEK cells following SPION exposure. No treatment (**a**), MicroMod SPION 20 nm (**b**) and 50 nm (**c**), KTH SPION 15 nm (**d**), and 20 nm (**e**). Conditions: HEK cells were grown to 70 % confluency in 25-cm^2 flasks and exposed to 26 μg/cm^2 of SPION for 24 h. The HEK were harvested with trypsin/EDTA, rinsed in HBSS, and fixed with Trump's fixative

the HEK (Fig. 3b, c). An electron translucent matrix similar to that noted in the native prep was occasionally present in cells treated with the 20 nm colloid (Fig. 3b). The KTH SPION agglomerates were found in the cellular vacuoles of isolated cells as well as discrete agglomerates which were sometimes located within the cell cytoplasm. (Fig. 3d, e). Overall, the exposed cells contained vacuoles but otherwise appeared healthy.

Release of Inflammatory Cytokines by HEK Following Exposure to SPION

Inflammatory cytokine, IL-6, IL-8, IL-1β, IL-10, and TNF-α, release from HEK cells was analyzed in the supernatant following exposure to SPION for 24 h. KTH SPION (15 and 20 nm) induced a significant 4.25- and 3.25-fold increase in IL-8 release, respectively, while only 50 nm MicroMod SPION induced a significant (1.5-fold) release of IL-8 (Fig. 4a). IL-6 release was significantly increased (1.6-fold) by exposure to 15 nm KTH SPION, while both 20 and 50 nm MicroMod SPION were capable of significantly inducing elevated levels (1.6- and 1.9-fold, respectively) of IL-6 (Fig. 4b). IL-1β, IL-10, and TNF-α levels were below detectable levels in the samples evaluated.

Effect of SPIONs on Cell Viability, Cell Damage, and Oxidative Stress in JB6 P$^+$ Cells

Cytotoxicity was evaluated in mouse epidermal cells (JB6 P$^+$ cells) following exposure to MicroMod SPION (20 and 50 nm) or KTH (15 and 20 nm) for 24 h with or without UVB pre-treatment. MicroMod (20 nm; Fig. 5a) or KTH (15 and 20 nm; Fig. 5c, d) alone were not cytotoxic to JB6 P$^+$ cells at the doses evaluated (2.6, 5.2, 13, and 26 μg/cm^2). Exposure to MicroMod SPION (50 nm) alone resulted in a significant 5 % reduction in cell viability at the highest dose evaluated (26 μg/cm^2) (Fig. 5b). Co-exposure with UVB and 26 μg/cm^2 MicroMod (20 and 50 nm) or KTH (15 nm) SPION led to a significant (11, 6, or 11 %, respectively) reduction in viability of JB6 P$^+$ cells; however, these results were not greater than the effects observed from the individual exposures.

LDH activity was evaluated in JB6 P$^+$ cell cultures as an assessment of cellular damage following SPION exposure

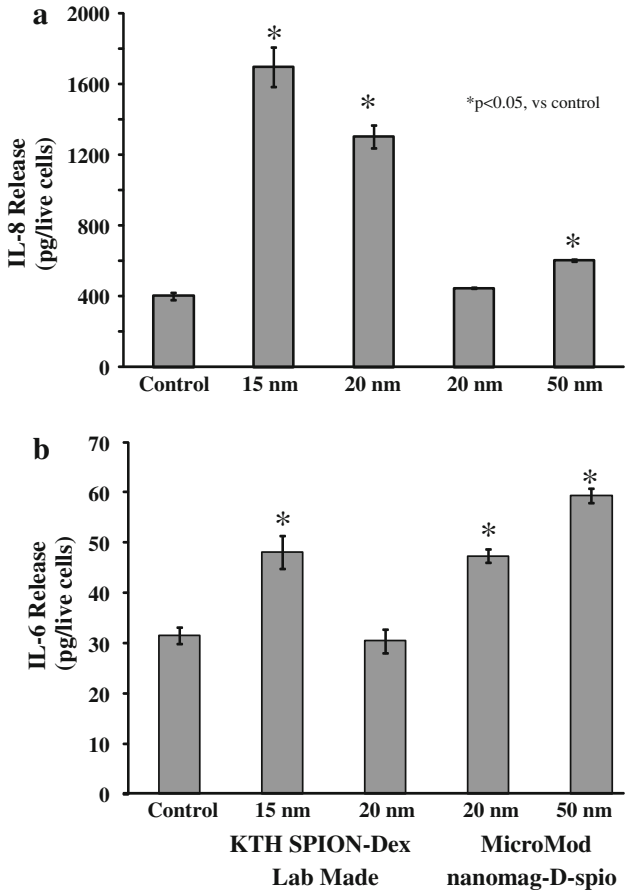

Fig. 4 Inflammatory cytokine release from HEK following exposure to SPION: IL-8 (**a**), IL-6 (**b**). Conditions: HEK cells were grown to 70 % confluency in 25-cm^2 flasks and exposed to 26 μg/cm^2 of SPION ($n = 6$ wells/treatment) for 24 h. After exposure, cellular supernatant was collected and inflammatory cytokines were measured. Significance indicated by $*p < 0.05$ versus control

with or without UVB pre-treatment. Both sizes (15 and 20 nm) of KTH SPION particles alone induced a significant 2- and 2.5-fold increase, respectively, in the release of LDH following exposure to 26 μg/cm^2, while exposure to MicroMod SPION (20 and 50 nm) alone did not result in LDH release (Fig. 6). UVB exposure alone was sufficient to induce a significant 17-fold increase in the release of LDH compared non-UVB-treated control. The combined effect of UVB and KTH SPION (15 and 20 nm) also resulted in significant (1.2- and 1.5-fold, respectively), synergistic, and size-dependent increase in the release of LDH as compared to UVB control as well as a 8.6- and 6.7-fold increase, respectively, in LDH versus non-UVB SPION-treated cells. Co-exposure to UVB and MicroMod SPION (20 and 50 nm) did not lead to detectable levels of LDH above that observed in cells treated with UVB alone.

In order to determine the cellular redox status of JB6 P$^+$ cells following exposure to SPION with or without UVB pre-treatment, the level of GSH in the cells was evaluated. The addition of ThioGlo-1™ to cell homogenates produces an instantaneous increase in fluorescence as a result of the formation of GSH–ThioGlo-1™ reaction products. As shown in Fig. 7a, 20 nm MicroMod SPION alone induced a significant 10–20 % reduction (2.6–13 μg/cm^2) in the level of GSH in JB6 P$^+$ cells while 50 nm MicroMod SPION (Fig. 7b) alone did not induce oxidative stress as evidenced by no changes in GSH levels. KTH SPION (15 nm; Fig. 7c) alone induced a dose-dependent (30–60 %) decrease in GSH levels following exposure to 2.6–26 μg/cm^2, respectively. 20 nm KTH SPION (Fig. 7d; 2.6–26 μg/cm^2) alone also induced a dose-dependent (20–50 %, respectively) decrease in GSH levels. UVB alone was not sufficient to induce reduction in GSH levels in JB6 P$^+$ cells. Pre-exposure to UVB followed by MicroMod SPION (20 and 50 nm) had no effect of the level of GSH in JB6 P$^+$ cells (Fig. 7a, b). KTH SPION (15 nm)-treated cells pre-exposed to UVB exhibited a more profound reduction (60 % vs. UVB control and 20 % vs. non-UVB exposed SPION-treated cells) in GSH levels only at the highest concentration evaluated (26 μg/cm^2; Fig. 7c). The combined effect of UVB and KTH SPION (20 nm) also resulted in significant (32–42 %) reduction in GSH levels as compared to UVB control at all the concentrations evaluated (2.6–26 μg/cm^2, respectively) as well as a 20 (2.6 μg/cm^2) and 25 % (5.2–26 μg/cm^2) decrease in GSH versus non-UVB SPION-treated cells (Fig. 7d).

Activation of AP-1 in JB6 P$^+$ Following Exposure to SPION

Activation of AP-1 was assessed in JB6 P$^+$ cells exposed to 0, 2.6, 5.2, or 26 μg/cm^2 MicroMod SPION (20 and 50 nm) or KTH SPION (15 and 20 nm) for 24 h. Exposure of JB6 P$^+$ cells to KTH SPION particles resulted in a size- and dose-dependent increase in AP-1 activity. KTH SPION (15 nm) alone induced a dose-dependent 26, 47.5, and 83 % increase in AP-1 activity versus control following exposure to 2.6, 5.2, and 26 μg/cm^2 SPION, respectively, while a significant induction of AP-1 activity (44 and 55 %, respectively, vs. control) was observed following exposure to 2.6 and 26 μg/cm^2 of 20 nm KTH SPION alone (Table 2). MicroMod SPION alone induced a similar size-dependent response with 20 nm particles resulting in significant (35–46 %) AP-1 induction at all doses evaluated (2.6–26 μg/cm^2), while 50 nm particles significantly (16–27 %) induced AP-1 when exposed only to 5.2 and 2.6 μg/cm^2, respectively. UVB alone caused a significant activation of AP-1. Pre-treatment with UVB followed by exposure to 15 nm KTH SPION did not result in a significant activation of AP-1 as compared to UVB control (Table 2), while 20 nm KTH SPION (26 μg/cm^2) with UVB induced a significant increase (40 %, vs. UVB

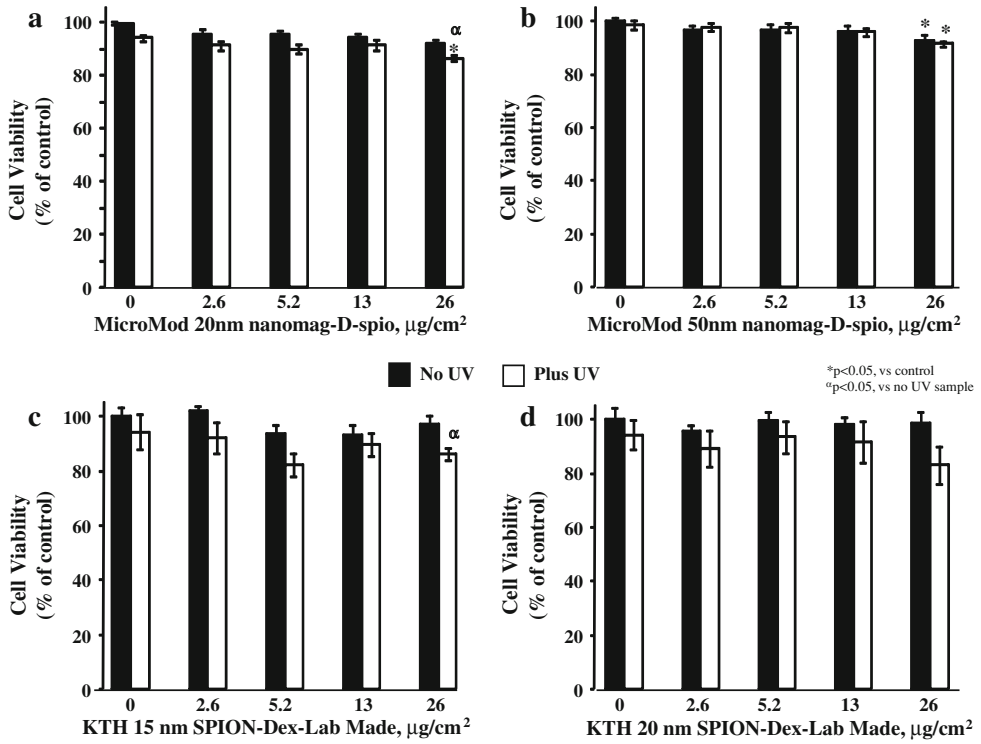

Fig. 5 Viability of JB6 P^+ cells following exposure to SPION with or without UVB pre-treatment: MicroMod 20 nm (**a**), MicroMod 50 nm (**b**), KTH 15 nm (**c**), KTH 20 nm (**d**). Conditions: prior to NP exposure, one group of JB6 P^+ cells (1×10^6) were exposed to 4 kJ/m^2 UVB radiation in MEM without phenol red and another group of cells remained under normal growth conditions in MEM without phenol red. Following UVB exposure, cells were incubated in phenol-free MEM with 2.6, 5.2, 13, or 26 μg/cm^2 for 24 h at 37 °C. After the incubation, cells were washed twice with PBS (pH 7.4) and then cell viability was determined with 10 % alamar Blue. Values are means ± SEM of three experiments. Significance indicated by $^*p < 0.05$ versus control, $^{\alpha}p < 0.05$ versus non-UVB exposed cells

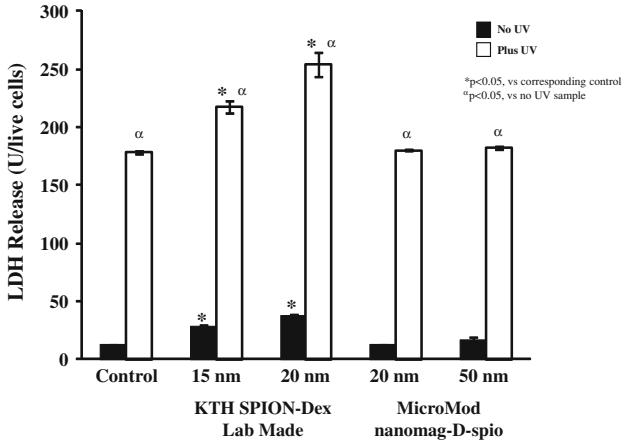

Fig. 6 Release of LDH by JB6 P^+ cells following exposure to SPION with or without UVB pre-treatment. Conditions: prior to NP exposure, one group of JB6 P^+ cells (1×10^6) were exposed to 4 kJ/m^2 UVB radiation in MEM without phenol red and another group of cells remained under normal growth conditions in MEM without phenol red. Following UVB exposure, cells were incubated in phenol-free MEM with 2.6, 5.2, 13, or 26 μg/cm^2 for 24 h at 37 °C. After the incubation, cells were washed twice with PBS (pH 7.4) and then cell viability was determined with 10 % alamar Blue. Values are means ± SEM of three experiments. Significance indicated by $^*p < 0.05$ versus corresponding control, $^{\alpha}p < 0.05$ versus non-UVB exposed cells

control) in AP-1 activity following exposure. The combined effect of UVB and MicroMod SPION on AP-1 activation was greater than the sum of the individual effects of SPION and UVB exposure (Table 2).

Activation of NF-κB in JB6 P^+ Cells After Exposure to SPION

NF-κB is a redox-sensitive transcription factor, which is involved in the regulation of a number of inflammatory reactions [40–42]. We found that exposure to SPION (KTH 15 and 20 nm; MicroMod 20 nm) alone did not cause induction of NF-κB in JB6 P^+ cells. The only significant induction (1.4-fold increase vs. control) of NF-κB occurred following exposure to 5.2 μg/cm^2 MicroMod SPION (50 nm) alone (Table 3). UVB exposure alone was sufficient (89.5-fold increase vs. non-UV control) to induce activation of NF-κB. The combined effect of UVB and SPION exposure resulted in a further activation of NF-κB as compared to the sum of the individual effects. 15 nm KTH SPION (5.2 μg/cm^2) and UVB induced a significant synergistic activation of NF-κB with the combined effect greater than the effects observed from the individual

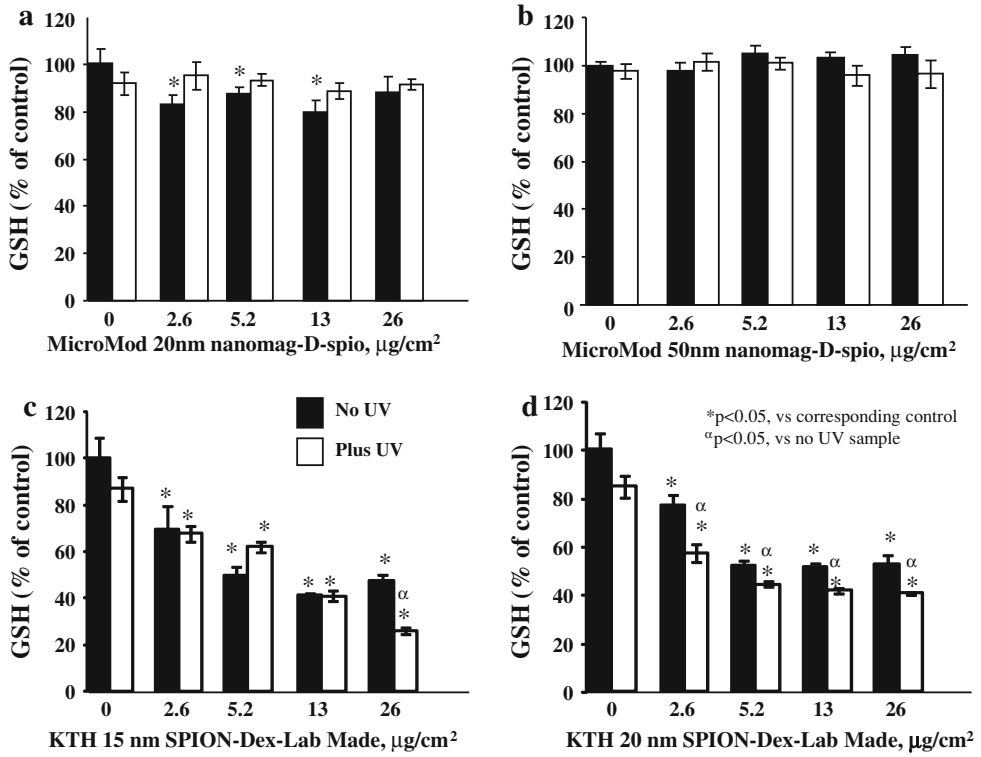

Fig. 7 GSH Levels in JB6 P^+ cells following exposure to SPION with or without UVB pre-treatment. MicroMod 20 nm (**a**), MicroMod 50 nm (**b**), KTH 15 nm (**c**), KTH 20 nm (**d**). Conditions: prior to NP exposure, one group of JB6 P^+ cells (1×10^6) were exposed to 4 kJ/m^2 UVB radiation in MEM without phenol red and another group of cells remained under normal growth conditions in MEM without phenol red. Following UVB exposure, cells were incubated in phenol-free MEM with 2.6, 5.2, 13, or 26 μg/cm^2 for 24 h at 37 °C. After the incubation, cells were washed twice with PBS (pH 7.4) and then cell viability was determined with 10 % alamar Blue. Values are means ± SEM of three experiments. Significance indicated by $^*p < 0.05$ versus corresponding control, $^\alpha p < 0.05$ versus non-UVB exposed cells

exposures. MicroMod 50 nm SPION exposed cells pre-treated with UVB showed a greater than additive activation of NF-κB (Table 3).

Release of Inflammatory Cytokines by JB6 P^+ Cells Following Exposure to SPION

Release of the inflammatory cytokines, IL-6, MCP-1, IFN-γ, TNF-α, and IL-12, was evaluated in the cellular supernatant following exposure to SPION with or without UVB pre-treatment. Release of TNF-α was slightly elevated following exposure to KTH SPION (15 and 20 nm) alone; however, the results were not significantly different from control cells. MicroMod SPION alone did not induce TNF-α release (Fig. 8a). KTH SPION (15 and 20 nm) alone induced a significant (57 and 63 % increase, respectively, vs. control) release of IL-6 from JB6 P^+ cells following exposure (Fig. 7b). MCP-1 levels were significantly increased (76 %) following exposure to KTH (15 and 20 nm) or MicroMod (20 nm) alone (Fig. 8c). Pre-exposure to UVB and then SPION did not result in an amplification of cytokine release (Fig. 8). IL-12 and IFN-γ levels were below detectable levels in the samples evaluated.

Discussion

Increased use of NPs for a number of applications has led to a need to understand and evaluate their toxicity. Superparamagnetic iron oxide NPs have a number of applications in the biomedical field from use as an MRI contrast agent to potential carriers for drug delivery. A variety of published reports have evaluated the biocompatibility of SPION particles in a variety of cells, i.e., macrophages [43], endothelial [15], and fibroblasts [26, 27]. Investigations of the effects of SPION on keratinocytes and epidermal cells are limited.

Surface modification of SPION has been utilized to tailor the functional properties of the NP for a wide variety of clinical applications [8, 9]. These surface modifications affect the rate and ability of cells to engulf particles. Uncoated SPION are recognized by fibroblasts and

Table 2 Relative AP-1 activation ($\times 10^3$) in JB6 cells following exposure to dextran-coated SPION with or without UVB pre-treatment

SPION (μg/cm^2)	Non-UV				Plus UV			
	0	2.6	5.2	26	0	2.6	5.2	26
KTH SPION-dex lab made, 15 nm	18.36 ± 1.88	23.16 ± 0.72	27.09 ± 2.21*	33.56 ± 3.86*	778.6 ± 49.8*	863.8 ± 32.0	788.8 ± 36.5	948.2 ± 890
KTH SPION-dex lab made, 20 nm	18.36 ± 1.88	26.40 ± 2.20*	17.70 ± 1.90	28.51 ± 1.58*	778.6 ± 81.7*	691.5 ± 26.2	756.9 ± 60.3	1093.1 ± 87.2*
20 nm MicroMod nanomag-D-SPIO	18.36 ± 0.44	26.90 ± 0.87*	24.90 ± 0.39*	25.30 ± 1.55*	778.6 ± 22.4*	927.5 ± 33.0*	945.2 ± 63.2*	963.0 ± 11.0*
50 nm MicroMod nanomag-D-SPIO	18.86 ± 0.49	25.40 ± 4.57	21.84 ± 0 08*	23.88 ± 2.14*	715.5 ± 24.6*	795.9 ± 48.1	990.4 ± 42.5*	998.6 ± 36.3*

* $p < 0.05$ vs corresponding control

Table 3 Relative NF-κB activation ($\times 10^2$) in JB6 cells following exposure to dextran-coated SPION with or without UVB pre-treatment

SPION (μg/cm^2)	Non-UV				Plus UV			
	0	2.6	5.2	26	0	2.6	5.2	26
KTH SPION-dex lab made, 15 nm	4.18 ± 0.38	4.78 ± 0.25	4.50 ± 0.15	4.76 ± 0 18	376.2 ± 100.1*	1245.9 ± 400.2	2718.2 ± 801.4*	2302.0 ± 989.4
KTH SPION-dex lab made, 20 nm	4.18 ± 0.38	3.31 ± 0.14	3.59 ± 0.33	3.31 ± 0.13	376.2 ± 100.1*	931.6 ± 208.2*	1765.3 ± 573.7*	845.5 ± 28.9*
20 nm MicroMod nanomag-D-SPIO	4.18 ± 007	3.86 ± 0.18	3.97 ± 0.13	4.50 ± 0.38	376.0 ± 7.8*	355.8 ± 13.5	437.6 ± 25.7*	362.1 ± 26.5
50 nm MicroMod nanomag-D-SPIO	4.24 ± 0.08	5.17 ± 0.48	6.12 ± 0.18*	3.91 ± 0.12	371.3 ± 12.5*	403.1 ± 33.5	431.3 ± 7.4*	533.7 ± 29.6*

* $p < 0.05$ vs corresponding control

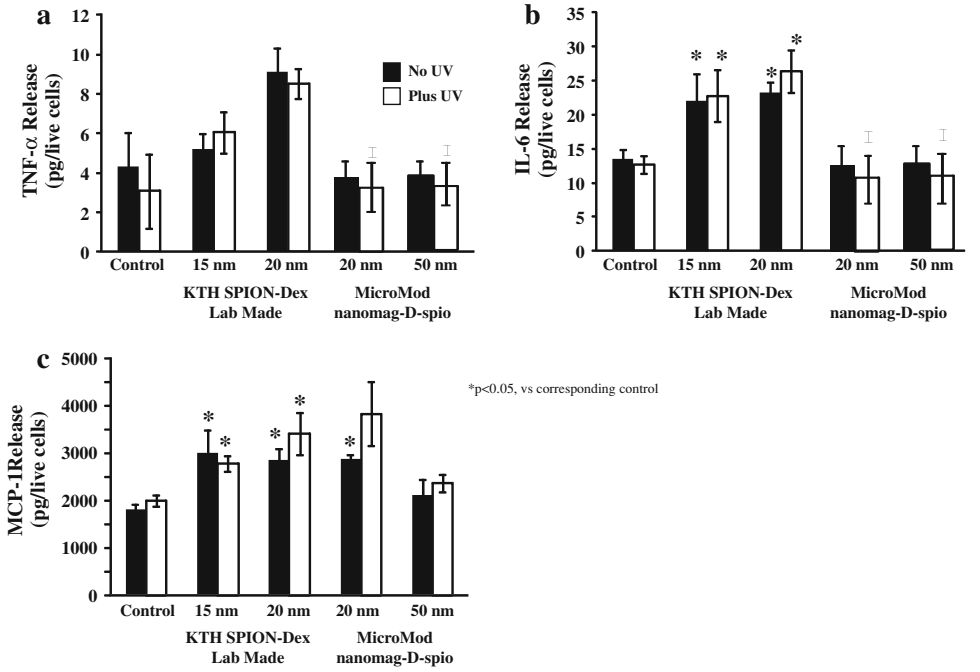

Fig. 8 Inflammatory cytokine release by JB6 P^+ cells following SPION exposure with or without UVB pre-treatment: TNF-α (**a**), IL-6 (**b**), MCP-1 (**c**). Conditions: prior to NP exposure, one group of JB6 P^+ cells (1×10^6) were exposed to 4 kJ/m^2 UVB radiation in MEM without phenol red and another group of cells remained under normal growth conditions in MEM without phenol red. Following UVB exposure, cells were incubated in phenol-free MEM with 2.6, 5.2, 13, or 26 μg/cm^2 for 24 h at 37 °C. After the incubation, cells were washed twice with PBS (pH 7.4) and then cell viability was determined with 10 % alamar Blue. Values are means ± SEM of three experiments. Significance indicated by $^*p < 0.05$ versus corresponding control, $^{\alpha}p < 0.05$ versus non-UVB exposed cells

endocytosed into vacuoles within cells [26, 27, 44] and result in disruption of cellular cytoskeleton and decreased cellular proliferation [26, 27]. PEG-modified SPION are more readily engulfed by fibroblasts [44], while albumin-modified are not readily engulfed by cells and induce cellular proliferation [27]. Dextran-coated SPION are capable of being internalized by a number of primary as well as tumor cells in concentrations ranging from 0.011 to 0.118 pg/cell with peritoneal macrophages engulfing up to 0.97 pg [15, 45, 46]. In line with published reports, the KTH SPION (15 and 20 nm) evaluated in our study were found in vacuoles of HEK; however, the MicroMod SPION (20 and 50 nm) were not internalized by HEK cells.

Excessive exposure to ultraviolet light can cause both acute and chronic skin damage [29]. Acute dermal exposure to ultraviolet light has a variety of side effects known as erythema, inflammation, and/or sunburn, while chronic UV exposure can cause pigmentary changes, pre-mature photoaging, and an increased risk for the formation of cutaneous melanoma and non-melanoma skin cancers [47–49]. Short-term exposure to low-dose UV radiation has been shown to result in the formation of ROS [30, 50, 51].

The presence and the formation of ROS is able to damage biomolecules [52] during cellular oxidative stress [51]. It has also been demonstrated that UV-light-induced ROS were also able to cause structural and functional alterations in cutaneous proteins, e.g., collagen, elastin, and glycosaminoglycans, probably contributing to dermal phototoxicity and photoaging of the skin [53]. In this study, to evaluate the combine effect of UVB and SPION, JB6 cells were exposed to 4 kJ/m^2 UVB prior to SPION exposure. The dose of UVB utilized in this study was sufficient to induce cell damage (LDH release) as well as AP-1 and NF-κB but did not induce cell death.

The reported low toxicity and long half-life of dextran-modified SPION have made them a NP of particular interest for biological applications [15, 54]. Internalization of dextran-coated SPION can result in the dextran shell of the particles being broken down leading to the formation of particle chains/aggregates within the cell capable of inducing alterations in cellular processes. The presence of dextran-coated SPION within the cell may also induce oxidative stress via production of ROS. Due to the magnetic properties of SPION, direct measurement of radical production by electron spin resonance was not possible. In order to evaluate ROS production following SPION exposure, measurements of oxidative stress, specifically GSH, were utilized. A complex antioxidant defense system in the cells is present to detoxify ROS via the reduction of antioxidants. The presence of intracellular thiols within the antioxidant network has been shown to inhibit cytokine production. Specifically, GSH is an important sulfur-

containing antioxidant, which maintains the intracellular redox status by efficiently regulating the cellular defenses protecting against the development of oxidative stress by directly scavenging ROS [55–62]. In line with this, we found dose-dependent decreases in GSH levels in mouse epidermal cells following exposure to KTH SPION particles (15 and 20 nm), indicating the occurrence of oxidative stress as a result of exposure. An additive dose-dependent reduction in GSH level (up to 42 %) was found after combined exposure to UVB and KTH SPION (20 nm).

The cellular depletion of GSH has been shown to increase ROS formation, thereby resulting in enhanced cytokine secretion [63]. The generation of free radicals and subsequent oxidative stress are considered to be the central pathway involved in the development of a variety of skin disorders, such as photosensitivity and phototoxicity, photoaging, carcinogenesis, and cutaneous autoimmune diseases [64–66].

Changes in redox state of the cell due to overproduction of ROS results in induction of AP-1 and NF-κB [67–69]. AP-1 activation occurs via the upregulation of protein kinase C in response to oxidant exposure [70–72], while activation of NF-κB occurs due to ROS acting as a second messenger [73, 74]. In this study, AP-1 but not NF-κB activation occurred following SPION exposure alone. The combined effect of UVB and KTH SPION exposure significantly induced NF-κB, while the AP-1 response was additive due to very high activation from UVB alone.

Upregulation of NF-κB and AP-1 has been shown to cause an increase in the production of a number of inflammatory cytokines and chemokines, including IL-1, IL-6, IL-8, TNF-α, MCP-1, MIP-1α, MIP-2, COX-2 and iNOS, which are responsible for the development of a variety of disease states [40–42]. IL-8, IL-6, and IL-1 have been implicated in the development of dermal irritation [75–78]. Keratinocytes release TNF-α and IL-1β in response to acute tissue injury or inflammation. Release of IL-8, which plays a role in skin inflammatory disease [79], is stimulated by TNF-α and IL-1β. SPION and ultrasmall superparamagnetic iron oxide internalized by primary rat and murine macrophages were shown to be anti-inflammatory via release of IL-10 and a reduced production of inflammatory stimuli [43]. Dextran-coated SPION have been shown to decrease the phagocytic function of murine macrophages, while inducing an increase in the release of pro-inflammatory cytokines, i.e., TNF-α [80]. This study showed release of IL-8 and IL-6 by HEK cells following exposure to KTH SPION and MicroMod. Elevated levels of MCP-1 were secreted by JB6 cells in response to the smaller SPION particles alone, while the larger (50 nm) particle did not induce MCP-1 release. KTH SPION particles alone (15 and 20 nm) were also capable of significantly inducing IL-6. UVB alone or in co-exposure with SPION did not have an effect on release of the inflammatory cytokine evaluated.

Overall, the current results showed SPION-induced cytotoxicity and oxidative stress with induction of the redox-sensitive signal transduction pathways, AP-1 and NF-κB. Exposure to SPION alone, specifically the smaller NP evaluated (15 and 20 nm), caused oxidative stress via depletion of GSH, induction of AP-1, and release of pro-inflammatory mediators MCP-1 and IL-6. In conclusion, our data indicate that SPION exposure can cause size-dependent dermal induction of oxidative stress, activation of signal transduction pathways, and subsequent release of inflammatory mediators. The observed increased effects of combined exposure of UVB and SPION may be considered additive. However, considering the possibility of internalization of SPION particles by skin cells with no remarkable cytotoxic effect, accumulation of these particles in the skin may lead to cumulative effects and further investigation is needed.

Acknowledgments This work was supported by NIOSH OH008282, NORA 927Z1LU and the 7th Framework Program of the European Commission (EC-FP-7-NANOMMUNE-214281).

Disclaimer The findings and conclusions in this report are those of the author(s) and do not necessarily represent the views of the National Institute for Occupational Safety and Health.

References

1. Roco, M. C., Williams, S., & Alivisatos, P. (2000). *Nanotechnology research directions: IWGN workshop report*. Dordrecht: Kluwer.
2. Muller, K., Skepper, J. N., Posfai, M., Trivedi, R., Howarth, S., Corot, C., et al. (2008). Effect of ultrasmall superparamagnetic iron oxide nanoparticles (Ferumoxtran-10) on human monocyte-macrophages in vitro. *Biomaterials, 28*, 1629–1642.
3. Weissleder, R., Bogdanov, A., Neuwelt, E. A., & Papisov, M. (1995). Long-circulating iron oxides for MR imaging. *Advanced Drug Delivery Reviews, 16*, 321–324.
4. Reimer, P., & Weissleder, R. (1996). Development and experimental application of receptor-specific MR contrast media. *Radiology, 36*, 153–163.
5. Chouly, C., Pouliquen, D., Lucet, I., Jeune, J. J., & Jallet, P. (1996). Development of superparamagnetic nanoparticles for MRI: Effect of particle size, charge, and surface nature on biodistribution. *Journal of Microencapsulation, 13*, 245–255.
6. Jung, C. W., & Jacobs, P. (1995). Physical and chemical properties of superparamagnetic iron-oxide MR contrast agents-ferumoxides, ferumoxtran, ferumoxsil. *Magnetic Resonance Imaging, 13*, 661–674.
7. Corot, C., Robert, P., Idee, J. M., & Port, M. (2006). Recent advances in iron oxide nanocrystal technology for medical imaging. *Advanced Drug Delivery Reviews, 58*, 1471–1504.
8. Curtis, A. S. G., & Wilkinson, C. (2001). Nanotechniques and approaches in biotechnology. *Trends in Biotechnology, 19*, 97–101.
9. Moghimi, S. M., Humter, A. C. H., & Murray, J. C. (2001). Long-circulating and target-specific nanoparticles: Theory to practice. *Pharmacological Reviews, 53*, 283–318.

10. Chan, D. C. F., Kirpotin, D., & Bunn, P. A. (1993). Synthesis and evaluation of colloidal magnetic iron-oxides for the site-specific radiofrequency-induced hyperthermia of cancer. *Journal of Magnetism and Magnetic Materials, 122*, 374–378.
11. Mornet, S., Vasseur, S., Grasset, F., & Duguet, E. (2004). Magnetic nanoparticle design for medical diagnosis and therapy. *Journal of Materials Chemistry, 14*, 2161–2175.
12. Morawski, A. M., Lanza, G. A., & Wickline, S. A. (2005). Targeted contrast agents for magnetic resonance imaging and ultrasound. *Current Opinion in Biotechnology, 16*(1), 89–92.
13. Ziv-Polat, O., Topaz, M., Brosh, T., & Margel, S. (2010). Enhancement of incisional wound healing by thrombin conjugated iron oxide nanoparticles. *Biomaterials, 31*, 741–747.
14. Veiseh, O., Gunn, J. W., Kievit, F. M., Sun, C., Fang, C., Lee, J. S. H., et al. (2009). Inhibition of tumor-cell invasion with chlorotoxin-bound superparamagnetic nanoparticles. *Small (Weinheim an der Bergstrasse, Germany), 5*(2), 256–264.
15. Moore, A., Marecos, E., Bogdanov, A., & Weissleder, R. (2000). Tumoral distribution of long-circulating dextran-coated iron oxide nanoparticles in a rodent model. *Radiology, 214*, 568–574.
16. Huh, Y. M., Jun, Y. W., Song, H. T., Kim, S., Choi, J. S., Lee, J. H., et al. (2005). In vivo magnetic resonance detection of cancer by using multifunctional magnetic nanocrystals. *Journal of the American Chemical Society, 127*(35), 12387–12391.
17. Zhao, M., Beauregard, D. A., Loizou, L., Davletov, B., & Brindle, K. M. (2001). Non-invasive detection of apoptosis using magnetic resonance imaging and a targeted contrast agent. *Nature Medicine, 7*(11), 1241–1244.
18. Weissleder, R., Moore, A., Mahmood, U., Bhorade, R., Benveniste, H., Chiocca, E. A., et al. (2000). In vivo magnetic resonance imaging of transgene expression. *Nature Medicine, 6*(3), 351–355.
19. Jun, Y. W., Huh, Y. M., Choi, J. S., Lee, J. H., Song, H. T., Kim, S., et al. (2005). Nanoscale size effect of magnetic nanocrystals and their utilization for cancer diagnosis via magnetic resonance imaging. *Journal of the American Chemical Society, 127*(16), 5732–5733.
20. Bulte, J. W., Douglas, T., Witwer, B., Zhang, S. C., Strable, E., Lewis, B. K., et al. (2001). Magnetodendrimers allow endosomal magnetic labeling and in vivo tracking of stem cells. *Nature Biotechnology, 19*(12), 1141–1147.
21. Van Beers, B. E., Pringot, J., & Gallez, B. (1995). Iron oxides as contrast agents for MRI of the liver. *Journal de Radiologie, 76*(11), 991–995.
22. Weissleder, R., Stark, D. D., Engelstad, B. L., Bacon, B. R., Compton, C. C., White, D. L., et al. (1989). Superparamagnetic iron oxide: Pharmacokinetics and toxicity. *American Journal of Radiology, 152*(1), 167–173.
23. Weissleder, R., Elizondo, G., Wittenberg, J., Rabito, C. A., Bengele, H. H., & Josephson, L. (1990). Ultrasmall superparamagnetic iron oxide: Characterization of a new class of contrast agents for MR imaging. *Radiology, 175*, 489–493.
24. Wilhelm, C., Billotey, C., Roger, J., Pons, J. N., Bacri, J. C., & Gazeau, F. (2003). Intracellular uptake of anionic superparamagnetic nanoparticles as a function of their surface coating. *Biomaterials, 24*, 1001–1011.
25. Metz, S., Bonaterra, G., Rudelius, M., Settles, M., Rummeny, E. J., & Daldrup-Link, H. E. (2004). Capacity of human monocytes to phagocytose approved iron oxide MR contrast agents in vitro. *European Radiology, 14*, 1851–1858.
26. Berry, C. C., Wells, S., Charles, S., Aitchison, G., & Curtis, A. S. G. (2004). Cell response to dextran-derivatised iron oxide nanoparticles post internalisation. *Biomaterials, 25*, 5405–5413.
27. Berry, C. C., Wells, S., Charles, S., & Curtis, A. S. G. (2003). Dextran and albumin derivatised iron oxide nanoparticles: Influence on fibroblasts in vitro. *Biomaterials, 24*, 4551–4557.
28. Martin, A. L., Bernas, L. M., Rutt, B. K., Foster, P. J., & Gillies, E. R. (2008). Enhanced cell uptake of superparamagnetic iron oxide nanoparticles functionalized with dendritic guanidines. *Bioconjugate Chemistry, 19*, 2375–2384.
29. Miyachi, Y., & Imamura, S. (1990). Photo-oxidative skin damage and antioxidants. *Photodermatology Photoimmunology & Photomedicine, 7*, 49–50.
30. Jurkiewicz, B. A., & Buettner, G. R. (1994). Ultraviolet light-induced free radical formation in skin: An electron paramagnetic resonance study. *Photochemistry and Photobiology, 59*, 1–4.
31. Trouba, K. J., Hamadeh, H. K., Amin, R. P., & Germolec, D. R. (2002). Oxidative stress and its role in skin disease. *Antioxidants & Redox Signaling, 4*(4), 665–673.
32. Alder, V., Yin, Z., Tew, K. D., & Ronai, Z. (1999). Role of redox potential and reactive oxygen species in stress signaling. *Oncogene, 18*, 6104–6111.
33. Jordan, A., Wust, P., Scholz, R., Tesche, B., Fahling, H., Mitrovics, T., et al. (1996). Cellular uptake of magnetic fluid particles and their effects on human carcinoma cells exposed to AC magnetic fields in vitro. *International Journal of Hyperthermia, 12*(6), 705–722.
34. Dhar, A., Young, M. R., & Colburn, N. H. (2002). The role of AP-1, NF-kB and ROS/NOS in skin carcinogenesis: The JB6 model is predictive. *Molecular and Cellular Biochemistry, 234*(235), 185–193.
35. Colburn, N. H., Former, B. F., Nelson, K. A., & Yuspa, S. H. (1979). Tumour promoter induces anchorage independent irreversibility. *Nature, 281*, 589–591.
36. Colburn, N. H., & Lockyer, J. (1982). Phobol diester and epidermal growth factor receptors in 12-O-tetradecanoylphorbol-13-acetate-resistant and -sensitive mouse epidermal cells. *Cancer Research, 42*, 3093–3097.
37. Keane, R. W., Srinivasan, A., Foster, L. M., Testa, M. P., Ord, T., Nonner, D., et al. (1997). Activation of CPP32 during apoptosis of neurons and astrocytes. *Journal of Neuroscience Research, 48*, 168–180.
38. Monteiro-Riviere, N. A., Inman, A. O., & Zhang, L. W. (2009). Limitations and relative utility of screening assays to assess engineered nanoparticle toxicity in human cell line. *Toxicology and Applied Pharmacology, 234*, 222–235.
39. Shvedova, A. A., Kommineni, C., Jeffries, B. A., Castranova, V., Tyurina, Y. Y., Tyurin, V. A., et al. (2000). Redox cycling of phenol induces oxidative stress in human epidermal keratinocytes. *Journal of Investigative Dermatology, 114*, 354–364.
40. Driscoll, K. E., Carter, J. M., Hassenbein, D. G., & Howard, B. (1997). Cytokines and particle-induced inflammatory cell recruitment. *Environmental Health Perspectives, 105*(Suppl 5), 1159–1164.
41. Mossman, B. T., & Churg, A. (1998). Mechanisms in the pathogenesis of asbestosis and silicosis. *American Journal of Respiratory and Critical Care Medicine, 157*, 1666–1680.
42. Schins, R. P., & Borm, P. J. (1999). Mechanisms and mediators in coal dust induced toxicity: A review. *Annals of Occupational Hygiene, 43*, 7–33.
43. Siglienti, I., Bendszus, M., Kleinschnitz, C., & Stoll, G. (2006). Cytokine profile of iron-laden macrophages: Implications for cellular magnetic resonance imaging. *Journal of Neuroimmunology, 173*, 166–173.
44. Gupta, A. K., & Curtis, A. S. G. (2004). Surface modified superparamagnetic nanoparticles for drug delivery: Interaction studies with human fibroblasts in culture. *Journal of Materials Science, 15*, 493–496.
45. Moore, A., Weissleder, R., & Bogdanov, A. (1997). Uptake of dextran-coated monocrystalline iron oxides in tumor cells and macrophages. *Journal of Magnetic Resonance Imaging, 7*, 1140–1145.

46. Schulze, E., Ferrucci, J. T., Poss, K., Lapointe, L., Bogdanova, A., & Weissleder, R. (1995). Cellular uptake and trafficking of a prototypical magnetic iron oxide label in vitro. *Investigative Radiology, 30*, 604–610.
47. Fuchs, J., & Kern, H. (1998). Modulation of UV-light-induced skin inflammation by D-alpha-tocopherol and L-ascorbic acid: A clinical study using solar simulated radiation. *Free Radical Biology & Medicine, 25*, 1006–1012.
48. Kligman, L. H., & Kligman, A. M. (1986). The nature of photoaging: Its prevention and repair. *Photodermatology, 3*, 215–227.
49. Longstreth, J., de Gruijl, F. R., Kripke, M. L., Abseck, S., Arnold, F., Slaper, H. I., et al. (1998). Health risks. *Journal of Photochemistry and Photobiology B: Biology, 46*, 20–39.
50. Black, H. S. (1987). Potential involvement of free radical reactions in ultraviolet light- mediated cutaneous damage. *Photochemistry and Photobiology, 46*, 213–221.
51. Darr, D., & Fridovich, I. (1994). Free radicals in cutaneous biology. *Journal of Investigative Dermatology, 102*, 671–675.
52. Kvam, E., & Dhale, J. (2003). Pigmented melanocytes are protected against ultraviolet-A-induced membrane damage. *Journal of Investigative Dermatology, 121*, 564–569.
53. Carbonare, M. D., & Pathak, M. A. (1992). Skin photosensitizing agents and the role of reactive oxygen species in photoaging. *Journal of Photochemistry and Photobiology B: Biology, 14*, 105–124.
54. Babincova, M., Leszczynska, D., Sourivong, P., & Babinec, P. (2000). Selective treatment of neoplastic cells using ferritin-mediated electromagnetic hyperthermia. *Medical Hypotheses, 54*(3), 177–179.
55. Schafer, F. Q., & Buettner, G. R. (2001). Redox environment of the cell as viewed through the redox state of the glutathione disulfide/glutathione couple. *Free Radical Biology & Medicine, 30*, 1191–1212.
56. Sies, H. (1999). Glutathione and its role in cellular function. *Free Radical Biology & Medicine, 27*, 916–921.
57. Kohen, R., & Nyska, A. (2003). Oxidation of biological systems: Oxidative stress phenomena, antioxidants, redox reactions, and methods for their quantification. *Toxicologic Pathology, 30*(6), 620–650.
58. Haddad, J. J. (2000). Glutathione depletion is associated with augmenting a proinflammatory signal: Evidence for an antioxidant/pro-oxidant mechanism regulating cytokines in the alveolar epithelium. *Cytokines, Cellular & Molecular Therapy, 6*, 177–187.
59. Haddad, J. J. (2002). Science review: Redox and oxygen-sensitive transcription factors in the regulation of oxidant-mediated lung injury: Role for nuclear factor-kappa B. *Critical Care, 6*(6), 481–490.
60. Haddad, J. J. (2002). Antioxidant and prooxidant mechanisms in the regulation of redox(y)-sensitive transcription factors. *Cellular Signalling, 14*(11), 879–897.
61. Hudson, V. M. (2001). Rethinking cystic fibrosis pathology: The critical role of abnormal reduced glutathione (GSH) transport caused by CFTR mutation. *Free Radical Biology & Medicine, 30*, 1440–1461.
62. Petroff, M. G., Petroff, B. K., & Pate, J. L. (2001). Mechanisms of cytokine-induced death of cultured bovine luteal cells. *Reproduction, 121*, 753–760.
63. Gosset, P., Wallaert, B., Tonnel, A. B., & Fourneau, C. (1999). Thiol regulation of the production of TNF-α, IL-6, and IL-8 by human alveolar macrophages. *European Respiratory Journal, 14*, 98–105.
64. Lopez-Torres, M., Thiele, J. J., Shindo, Y., Han, D., & Packer, L. (1998). Topical application of a-tocopherol modulates the antioxidant network and diminishes ultraviolet-induced oxidative damage in murine skin. *British Journal of Dermatology, 138*, 207–215.
65. Halliwell, B., & Cross, C. E. (1994). Oxygen-derived species: Their relation to human disease and environmental stress. *Environmental Health Perspectives, 102*, 5–12.
66. Nackbar, F., & Korting, H. C. (1995). The role of vitamin E in normal and damaged skin. *Journal of Molecular Medicine, 73*, 7–17.
67. Meyer, M., Pahl, H. L., & Bauerle, P. A. (1994). Regulation of the transcription factor NF-kB and AP-1 by redox changes. *Chemico-Biological Interacttions, 91*, 91–100.
68. Abate, C., & Curran, T. (1990). Encounters with Fos and Jun on the road to AP-1. *Seminars in Cancer Biology, 1*, 19–26.
69. Toledano, M. B., & Leonard, W. J. (1991). Modulation of transcription factor NF-kappa B binding activity by oxidation-reduction in vitro. *Proceedings of the National Academy of Sciences of the United States of America, 88*, 4328–4332.
70. Boyle, W. J., Smeal, T., Defize, L. H., Angel, P., Woodgett, J. R., Karin, M., et al. (1991). Activation of protein kinase C decreases phosphorylation of c-Jun at sites that negatively regulate its DNA-binding activity. *Cell, 64*(3), 73–84.
71. Papavassiliou, A. G., Bohmann, K., & Bohmann, D. (1992). Determining the effect of inducible protein phosphorylation on the DNA-binding activity of transcription factors. *Analytical Biochemistry, 203*(2), 302–309.
72. Cerruti, P. A. (1989). Response modification in carcinogenesis. *Environmental Health Perspectives, 81*, 39–43.
73. Schreck, R., Reiber, P., & Baeuerle, P. A. (1991). Reactive oxygen intermediates as apparently widely used messengers in the activation of the NF-kappa-B transcription factor and HIV-1. *EMBO Journal, 10*(8), 2247–2258.
74. Schreck, R., & Baeuerle, P. A. (1991). A role for oxygen radicals as second messengers. *Trends in Cell Biology, 1*(2–3), 39–42.
75. Barker, J., Mitra, R., Griffiths, C., Dixit, V., & Nickoloff, B. (1991). Keratinocytes as initiators of inflammation. *Lancet, 337*, 211–214.
76. Corsini, E., & Galli, C. (1998). Cytokines and contact dermatitis. *Toxicology Letters, 102–103*, 277–282.
77. Grone, A. (2002). Keratinocytes and cytokines. *Veterinary Immunology and Immunopathology, 88*, 1–12.
78. Nickolof, B. (1991). The cytokine network in psoriasis. *Archives of Dermatological Research, 127*, 871–884.
79. Chabot-Fletcher, M., Breton, J., Lee, J., Young, P., & Griswold, D. (1994). Interleukin-8 production is regulated by protein kinase C in human keratinocytes. *Journal of Investigative Dermatology, 103*, 509–515.
80. Hsaio, J. K., Chu, H. H., Wang, Y. H., Lai, C. W., Chou, P. T., Hsieh, S. T., et al. (2008). Macrophage physiological function after superparamagnetic iron oxide labeling. *NMR in Biomedicine, 21*, 820–829.